Electron and positron channeling radiation from beryllium oxide

H. D. Dulman and R. H. Pantell
Department of Electrical Engineering, Stanford University, Stanford, California 94305

J. O. Kephart
IBM T. J. Watson Research Center, Yorktown Heights, New York 10598

B. L. Berman
Department of Physics, The George Washington University, Washington, D.C. 20052

H. Park
AT&T Bell Laboratories, Murray Hill, New Jersey 07974

S. Datz
Physics Division, Oak Ridge National Laboratory, Oak Ridge, Tennessee 37831

R. K. Klein
Advanced Micro Devices, Inc., Sunnyvale, California 94088

R. L. Swent
High Energy Physics Laboratory, Stanford University, Stanford, California 94305

Z.-H. Bian
Stanford Linear Accelerator Center, Menlo Park, California 94025
(Received 6 July 1992; revised manuscript received 16 February 1993)

We present experimental observations of planar and axial channeling radiation emitted by relativistic electrons and positrons traversing a BeO crystal. Values of thermal vibration amplitudes are obtained, and found to be in agreement with those obtained by other methods, namely, x-ray and neutron diffraction. The standard channeling-radiation theory matches correctly the observed radiation spectra when the particle is channeled along principal planes. Some of the planes with higher Miller indices give radiation spectra that can only be explained by the coupling of the particle wave function to neighboring axes or planes, or by population redistribution within the band.

I. INTRODUCTION

When a particle is injected into a crystal nearly parallel to a principal plane or axis of symmetry, the particle will undergo periodic motion in the plane perpendicular to the direction of injection. The particle is trapped in the crystal potential and said to be "channeled." If the de Broglie wavelength associated with the particle transverse motion is comparable to the interplanar distance, wave interference effects (and thus quantum mechanics) need to be considered. This is the case for electrons or positrons with incident kinetic energies below 100 MeV, our area of study.

The standard analysis of channeling radiation, starting with the Dirac equation and reducing it to the Schrödinger equation, gives us the transition energies, strengths, and linewidths of the resulting radiation.[1–8] Due to relativistic motion, the observed radiation in the forward direction consists of hard x-rays concentrated within a cone of half-angle $1/\gamma$, where γ is the ratio of the particle total energy to its rest energy. The radiation spectrum consists mainly of discrete channeling transition lines, along with a continuous background due to bremsstrahlung. These lines are broadened by several effects, particularly scattering-induced incoherence.

Because of the periodicity of the crystal potential in the transverse direction, the wave functions of the channeled particle are of Bloch type, characterized by a level n and by the crystal momentum κ. Inside the potential well, the lowest-lying energy levels are essentially momentum independent, while levels close to the top of the well show a significant dispersion, giving momentum-dependent transition energies and thus producing a broader spectrum.

Previous publications presented results for channeling radiation in cubic and zinc blende structures.[9–11] This paper presents a study of channeling radiation from a beryllium oxide (BeO) crystal. Due to its unusual crystal structure (see below), it provides a more stringent test of the continuum potential approximation. In addition, as the thermal vibration amplitudes were believed to be small,[12] somewhere between diamond and silicon, the

theoretical calculations suggested that the spectral linewidths would be small, which was, in fact, what we observed. This is an important feature if channeling radiation is to be considered as a quasimonochromatic source of x rays.

In this study, we compare the measured channeling-radiation spectra for electrons and positrons with theoretical predictions. We also determine values for the atomic thermal vibration amplitudes, in good agreement with the latest values reported in the literature, obtained by different methods. Finally, we discuss the experimental results and propose explanations for certain discrepancies observed in the radiation spectra for momentum-dependent energy levels.

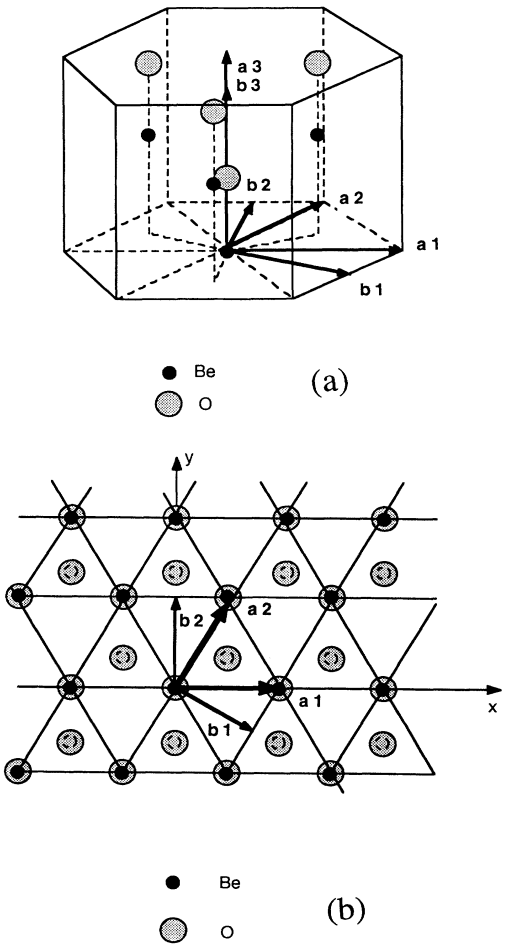

FIG. 1. Beryllium oxide (BeO) crystal structure (wurtzite). It consists of two hexagonal close-packed structures (one for Be and one for O), displaced in the $\mathbf{a}_3$ direction one from the other. Real $\{\mathbf{a}_i\}$ and reciprocal- $\{\mathbf{b}_j\}$ lattice vectors are indicated. (a) Three-dimensional view. The location of the atoms are Be_1, (0,0,0); Be_2, $(a/3, a/3, c/2)$; O_1, (0,0,vc); and O_2, $[a/3, a/3, (0.5+v)c]$, where $a=2.698$ Å, $c=4.38$ Å, and $v=0.378$. (b) Projection in the x-y plane. (This plane is parallel to the plane formed by the $\mathbf{a}_1$ and $\mathbf{a}_2$ vectors, as well as by the $\mathbf{b}_1$ and $\mathbf{b}_2$ vectors.)

II. STRUCTURE OF BERYLLIUM OXIDE

Beryllium oxide crystallizes into the wurtzite structure, space group $P6_3mc$.[13] Figure 1(a) shows a three-dimensional view of this crystal, while Fig. 1(b) shows its projection on the x-y plane. There are four atoms associated with each primitive cell, two of Be ($Z=4$) and two of O ($Z=8$); in the x-y plane, BeO forms a hexagonal structure.

There is relatively good agreement in the literature on the lattice dimensions for BeO, and we shall assume them to be correct. However, the literature presents a wide range of thermal vibration amplitudes. Various experimental probes, such as x-ray and γ-ray diffraction or neutron scattering, were used for these determinations, while multipole expansions, nonspherical electronic cloud distributions, and different ionicities were considered in some of the latest calculations.[12,14–18] Theoretical values were obtained using elastic constants and measured infrared or Raman frequencies.[12]

III. EXPERIMENTAL SETUP, DATA COLLECTION, AND PROCESSING

The experimental arrangement has been described in detail in the literature.[9,19] The accelerator used in this work was the 100-MeV electron-positron linear accelerator at the Lawrence Livermore National Laboratory. The pulse repetition rate was 1440 Hz, with a pulse duration of about 100 ns, while the beam current was adjusted so that the average counting rate at the detector was approximately 0.1 counts per beam burst, in order to limit pileup. This current is far below that required to heat or damage the crystal perceptibly. The 40-μm-thick BeO crystal was mounted on a three-axis goniometer. Crystal planes were located by noting orientations at which radiation enhancements occurred. After enough data points were obtained, a crystal map (see below) was obtained. Later, spectra were obtained at several of these crystal positions. The analysis of the crystal map and of the spectra allowed the identification of the planes.

The data were stored in the form of photon pulse-height spectra. The energy scale was calibrated with the use of radioactive sources (^{241}Am and ^{137}Cs, or ^{133}Ba). Random bremsstrahlung (BR) data were obtained for each channeling-radiation (CR) spectrum. To correct for the slight pileup, a pileup correction algorithm was applied to the data.[20]

The beam energy was determined approximately using a magnetic spectrometer. During the data processing, more accurate electron-beam energies were deduced as described below. For equal spectrometer readings, positron energies were taken to be equal to the deduced electron energies.

Several factors were considered in the spectral linewidth calculation. Even in a perfect crystal, an energetic electron will be scattered by small-impact-parameter collisions with the vibrating atomic nuclei, causing nonradiative transitions, and reducing the channeled particle's lifetime. This effect defines a coherence length, which in our case was calculated employing a

complex potential, the imaginary part of which causes scattering to other states, free or bound.[20–23] The resulting line shape is Lorentzian. The spectra were calculated at 201 points of the Brillouin zone, and later averaged assuming the particles to be equally distributed in κ space. Transitions with Δn up to 3 were included in the calculations. The resulting spectrum was successively convolved with Gaussian functions to take into account the energy spread, Doppler shift (due to the radiation cone and finite detector aperture), multiple scattering, and detector resolution. (Reference 11 contains an extensive analysis on how multiple scattering is taken into account, as well as a derivation of thermal vibration amplitudes for silicon. Other details are given in Refs. 4, 9, 10, and 20–23. A more sophisticated theory than the one we used can be found in Ref. 24 and references therein.)

In Sec. IV we present the experimental data and their theoretical fits, for planar channeling radiation of 17-, 30-, and 54-MeV electrons, and 54- and 83-MeV positrons in BeO. We start by presenting the crystal map, followed by the electron and positron channeling radiation data. In addition, some axial-channeling radiation spectra are presented. In Sec. V we discuss the experimental results. Thermal vibration amplitudes are obtained, and possible explanations for the disagreement between certain calculated and experimental spectra are given.

IV. EXPERIMENTAL DATA AND THEORETICAL FITS

A. Crystal map

Figure 2 shows a calculated crystal map that includes both the ⟨001⟩ and ⟨223⟩ axes. The many points are the angular positions of high index axes; planes are represented as nearly linear arrays of points. (Miller indices for both planes and axes are designated utilizing the convention for noncubic structures, as described in Ref. 25.) For most runs, the electron beam was injected nearly parallel to the ⟨223⟩ axis; in addition, during two runs, the crystal was rotated so that the beam was injected nearly parallel to the ⟨001⟩ axis, allowing more planes to be analyzed. Utilizing the angular location in (θ,φ) where data were collected (not shown) and the spectra, the various planes and axes were identified.

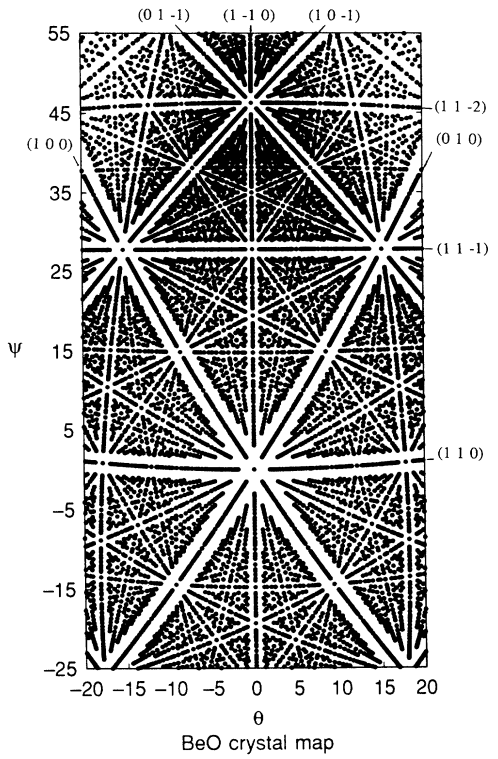

FIG. 2. Calculated crystal map. The principal planes have been indicated. Identification of main axes (in θ,ψ): ⟨001⟩=(0,0), ⟨101⟩≈(−15,28), ⟨011⟩≈(15,28), ⟨112⟩≈(0,28), ⟨111⟩≈(0,46), ⟨223⟩≈(0,35); the scales are in degrees.

B. Electron planar channeling-radiation data

Figures 3(a) and 3(b) show, respectively, the potential well $V(x)$ and the energy-momentum $E(\kappa)$ diagram for the (1−10) plane for an electron beam with $\gamma=60.22\pm0.15$. Figure 3(a) also presents (shadowed areas) the width of each energy band. Vertical lines indicate the position of the atomic planes. For this crystal orientation, Be and O atoms lie in the same plane. The higher-energy levels are crystal momentum dependent, i.e., their energy eigenvalues and eigenfunctions vary through the Brillouin zone, giving wider bands and thus wider radiative transition lines. Figure 3(c) shows the corresponding calculated channeling-radiation spectrum (solid line) superimposed on the experimental data points. The bremsstrahlung background has been subtracted. Note that the 3→2 transition gives a wider radiation line than those from deeply bound levels because of the Bloch broadening.

The thermal vibration amplitudes influence the potential well depth, affecting levels whose wave functions are concentrated close to the atomic planes, particularly the $n=0$ level. Hence, the beam energy can be deduced accurately by fitting the 2→1 transition, and then the thermal vibration amplitude by fitting the 1→0 transition. All other spectra at 30 MeV involve transitions to the $n=0$ level or too much Bloch broadening, and hence they cannot be used to determine the beam energy. A beam energy of $\gamma=60.22\pm0.15$ was deduced in this way. Figures 4 and 5 show the spectra for the same plane, respectively, for a $\gamma=106.90\pm0.30$ and 34.76 ± 0.16 electron beam. (The magnetic spectrometer gave, respectively, $\gamma=60.76$, 107.6, and 34.10.) A rms vibrational amplitude of 0.060 ± 0.006 Å for Be and 0.058 ± 0.0032 Å for O gives, with an uncertainty of ±0.5% in the 1→0 transition energy, the best fit at the analyzed electron energies. When the tolerance for one vibrational amplitude was estimated, the other was taken at the middle of its interval of validity. These values apply to vibrations in the x-y plane because channeling is insensitive to vibrations parallel to the channeling plane, and the (1−10) plane is parallel to the $\mathbf{a}_3$ (or $\mathbf{c}$) axis.

Figures 6 and 7 show the spectra for the (21−2) plane,

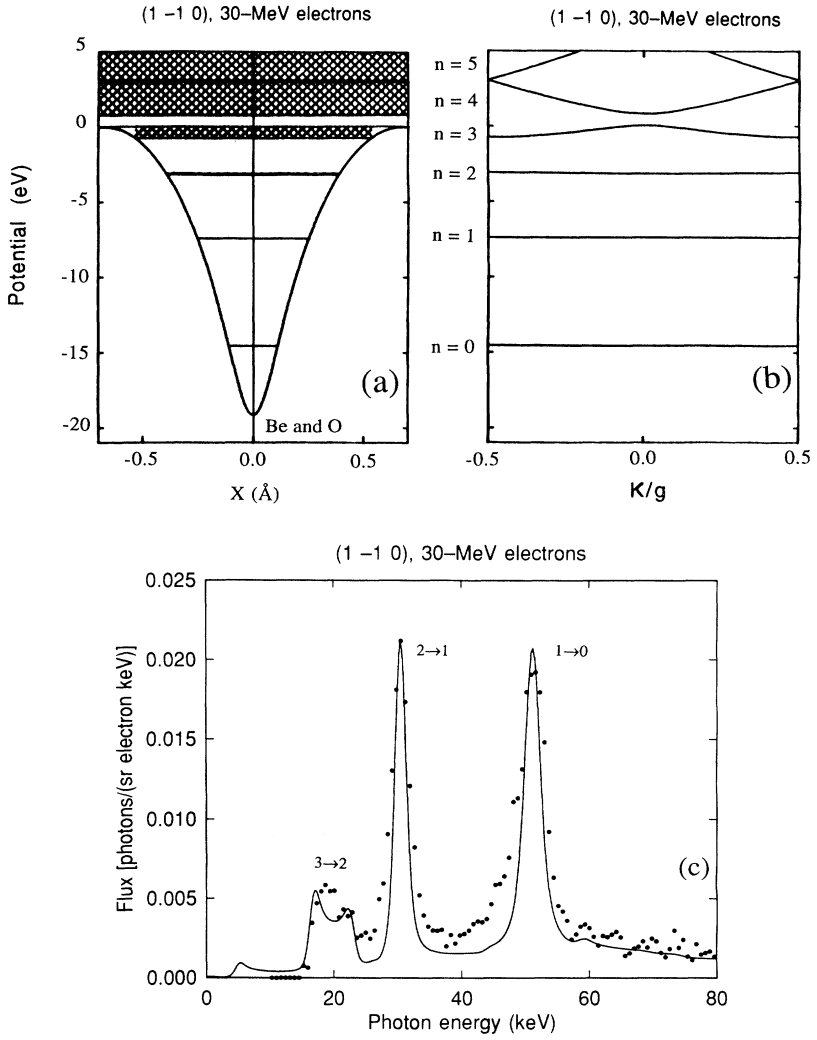

FIG. 3. 30-MeV ($\gamma = 60.22$) electrons channeled along the (1 − 10) plane of BeO. (a) Calculated interplanar potential and energy levels. Vertical line indicates the position of the atomic plane. Higher-energy levels are broadened in momentum space, due to the presence of neighboring atoms, thus giving an energy band [see also (b)]. (b) Energy vs momentum [$E(\kappa)$] dispersion diagram reduced to the first Brillouin zone; κ is the transverse crystal momentum and **g** the shortest reciprocal-lattice vector perpendicular to the channeling plane. (c) Channeling radiation spectrum; the dots represent the experimental data points, and the solid line represents the calculated spectrum.

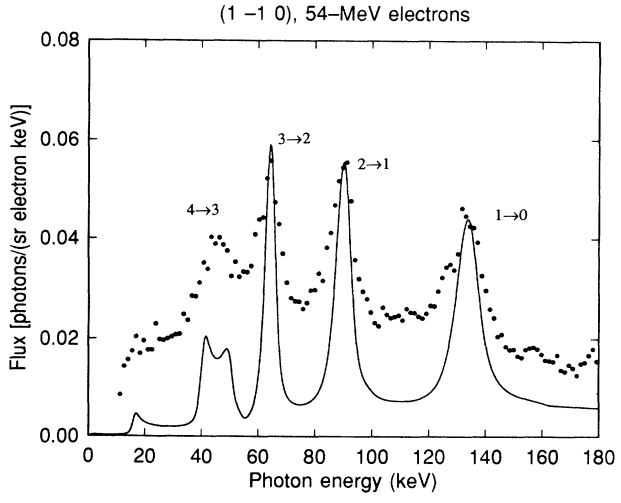

FIG. 4. 54-MeV ($\gamma = 106.9$) electrons channeled along the (1 − 10) plane. Experimental spectrum.

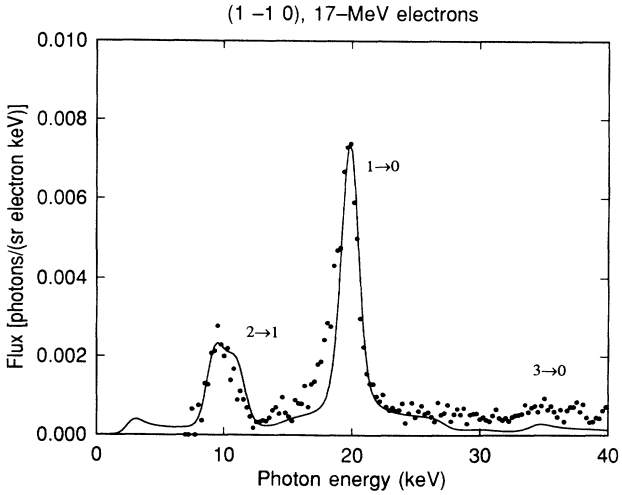

FIG. 5. 17-MeV ($\gamma = 34.76$) electrons channeled along the (1 − 10) plane. Experimental spectrum.

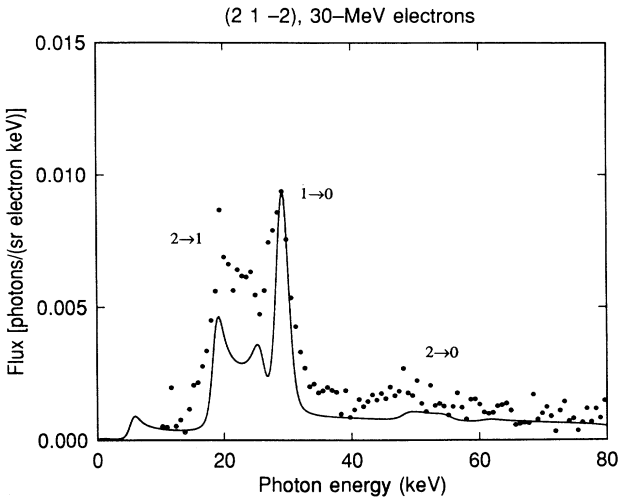

FIG. 6. 30-MeV ($\gamma=60.22$) electrons channeled along the (21−2) plane. Experimental spectrum.

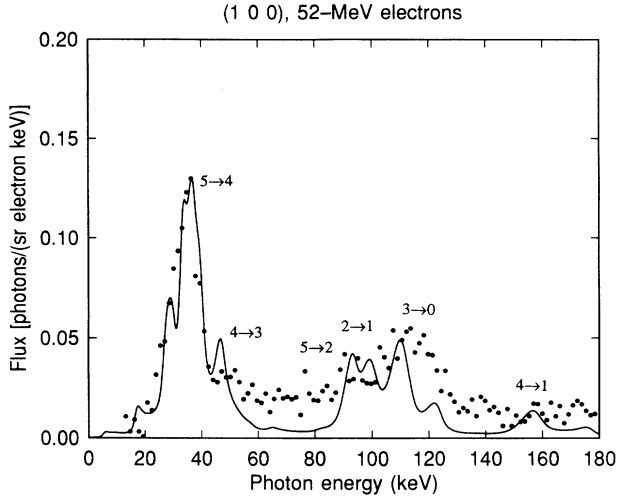

FIG. 8. 52-MeV ($\gamma=103.0$) electrons channeled along the (1 0 0) plane. Experimental spectrum.

at $\gamma=60.22$ and 106.9, respectively. The presence of a nonsymmetric well allows $2\rightarrow0$ transitions to exist.

The calculation of the thermal vibration amplitudes $\langle u^2\rangle^{1/2}$ in the $\mathbf{a}_3$ (or **c**) direction requires the plane to have a nonzero third Miller index. Utilizing the spectrum for this plane, as well as the one for the (22−3) plane, we obtain 0.070±0.025 Å for Be and 0.058±0.011 Å for O. (Values for $\langle u^2\rangle^{1/2}$ in the x-y plane were taken at the middle of their interval of validity.) The tolerances obtained are certainly large; this problem will also be addressed in Sec. V.

Figures 8–15 present spectral data from other planes where channeling radiation was observed. Note how even bumpy, asymmetric potential wells, such as the one shown in Fig. 10, can yield sharp spectral peaks. We comment on these results below. Table I contains our results for electron planar channeling radiation.

C. Positron planar channeling-radiation data

Figures 16(a) and 16(b) show, respectively, the potential well $V(x)$ and the energy-momentum $E(\kappa)$ diagram for the (1−10) plane for a positron beam with $\gamma=106.9\pm0.4$, while Fig. 16(c) shows the corresponding calculated channeling-radiation spectrum (solid line) superimposed on the measured experimental spectrum (data points). The best fit was obtained by taking the positron beam energy to be the same as for electrons, in agreement with the setting of the magnetic beam-energy analysis system.

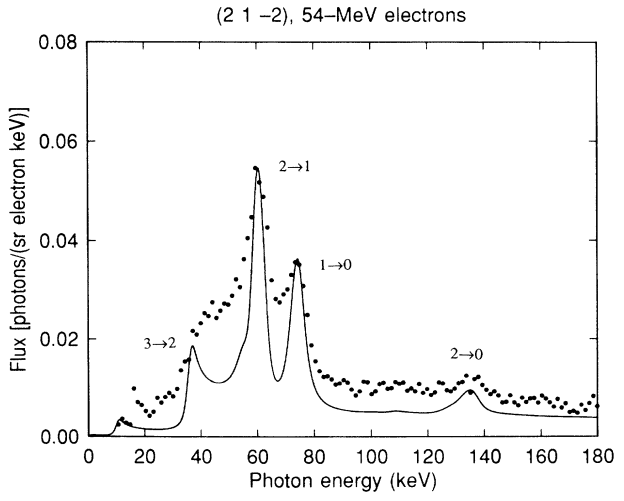

FIG. 7. 54-MeV ($\gamma=106.9$) electrons channeled along the (21−2) plane. Experimental spectrum.

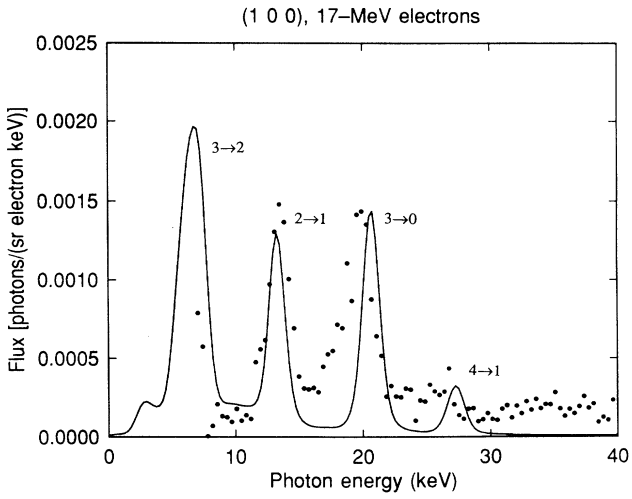

FIG. 9. 17-MeV ($\gamma=34.76$) electrons channeled along the (1 0 0) plane. Experimental spectrum.

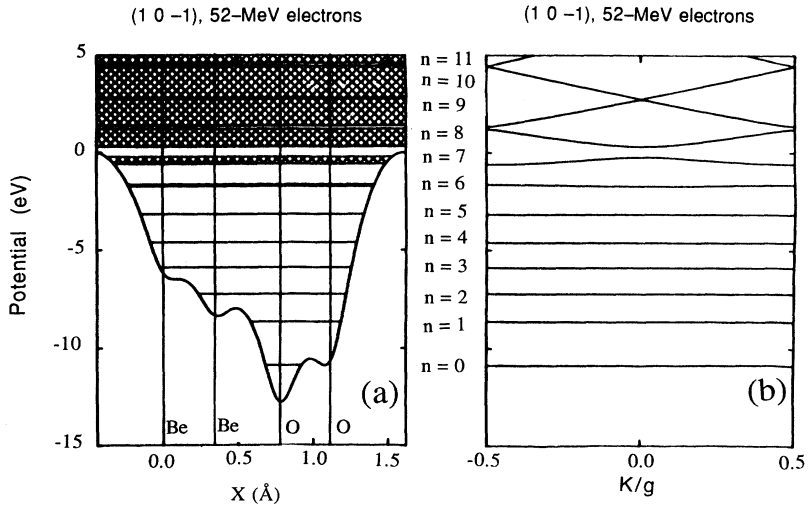

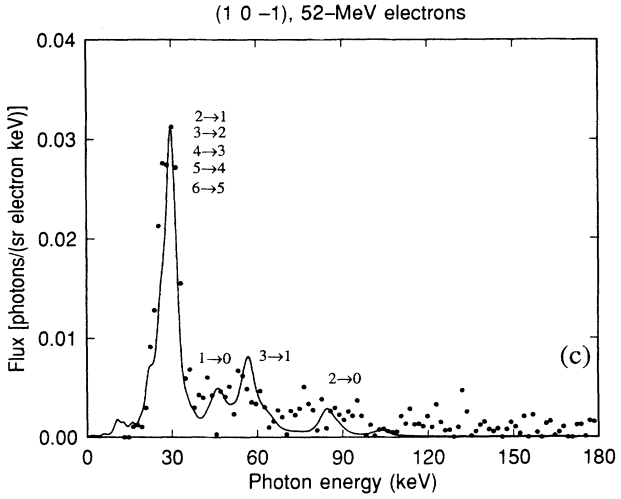

FIG. 10. 52-MeV ($\gamma = 103.0$) electrons channeled along the (10−1) plane. (a) Calculated interplanar potential and energy levels. Note that in spite of its bumpy, asymmetric form, spectral peaks occur. (b) Energy vs momentum [$E(\kappa)$] dispersion diagram reduced to the first Brillouin zone. (c) Channeling-radiation spectrum.

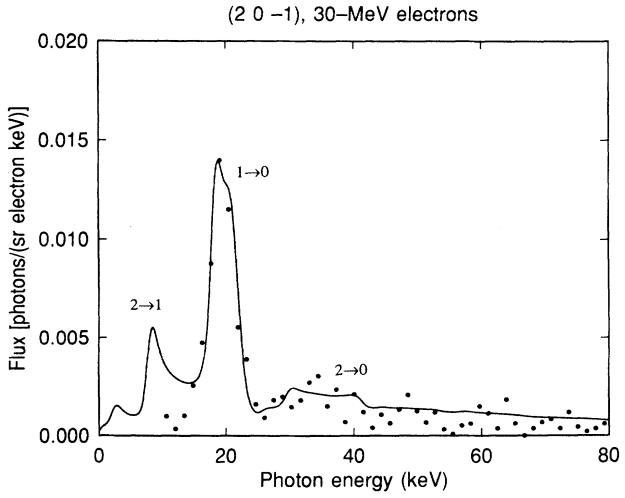

FIG. 11. 30-MeV ($\gamma = 60.22$) electrons channeled along the (20−1) plane. Experimental spectrum.

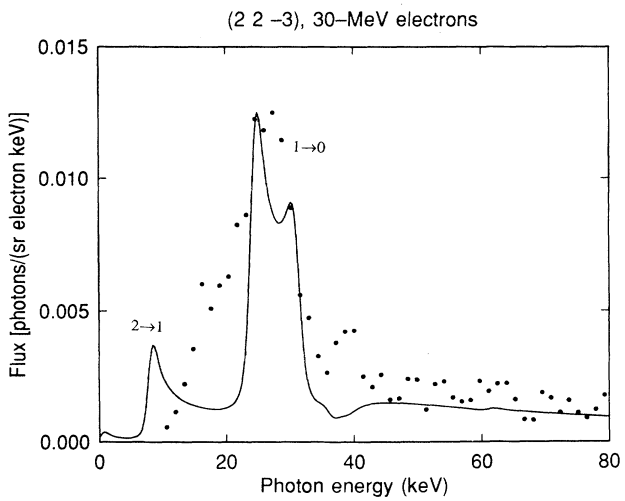

FIG. 12. 30-MeV ($\gamma = 60.22$) electrons channeled along the (22−3) plane. Experimental spectrum.

Figure 17 shows the spectrum for the same plane for positrons with $\gamma = 162.0 \pm 0.4$ (approximately 83 MeV). The magnetic spectrometer gave, respectively, $\gamma = 107.6$ and 163.7. For 83 MeV, electron runs were not performed, so γ was deduced from the best fit to the positron peak. The agreement between theoretical and experimental line shapes is excellent. The difference between the nominal beam energies obtained from the magnetic spectrometer reading and those obtained from fitting the channeling-radiation data is on the order of 1% in most cases. The discrepancy could arise from several sources, including slight miscalibration of the magnetic spectrometer and slight misalignment of the photon detector (causing it to see Doppler-shifted photon energies, which would lower the estimated beam energy). Use of the (higher) nominal beam energies and a failure to account properly for multiple scattering and other such corrections might contribute to an explanation of the significant discrepancies that we have previously noted between theoretical and experimental spectra from channeled positrons, but a definitive explanation requires further experimental work.[9]

Figures 18–22 present spectral data from other planes where positron-channeling radiation was also observed. Table II shows our results for positron planar channeling radiation.

TABLE I. Peak energies and linewidths of the electron-channeling-radiation spectra. Transitions from levels at the top of the well give broad lines, and in these cases the peak values are listed in parentheses. Linewidths are the full width at half maximum, for each transition. There is generally good agreement between the calculated and measured photon energies, and moderate agreement for the linewidths.

Plane and beam energy (MeV)	Transition	Calculated photon energy (keV) ±0.25 keV	Observed photon energy (keV) ±0.4 keV	Calculated linewidth (keV) ±0.25 keV	Observed linewidth (keV) ±0.4 keV
(1−10)					
17	1→0	19.8	19.6[a]	2.0	2.1
	2→1	(9.6)	9.7[b]	3.3	2.4
30	1→0	51.2	51.2	3.3	4.9
	2→1	30.6	30.6	2.1	3.2
	3→2	(17.0)	18.8	7.5	6.0
54	1→0	133.8	132.8[b]	8.5	11.4[c]
	2→1	90.0	90.0	7.3	8.6
	3→2	64.3	64.3	4.5	8.6
	4→3	(41.5)	45.5	11.3	14.3
(21−2)					
30	1→0	29.1	28.9	2.5	5.6
	2→1	(19.2)	19.4	8.8	7.0
54	1→0	74.3	73.9	6.8	9.8[c]
	2→1	60.5	60.5	6.5	12.7[c]
	2→0	134.9	135.8	7.0	10.0
(100)					
17	2→1	13.3	13.6[a]	1.6	2.0
	3→0	20.7	20.0	1.8	2.3
52	3→0	109.8	111.0	10.5	20.0
	5→4	36.6	36.5	12.8	10.4
(10−1)					
52	2→1[d]	29.8	30.5	6.3	8.2
(20−1)					
30	1→0	18.8	19.4	4.8	4.0
(22−3)					
30	1→0	25.0	27.0	7.8	9.8
54	1→0	71.2	70.4	8.0	17.6[c]
(32−3)					
30	1→0	(18.0)	18.7	5.5	7.0
54	1→0	(55.2)	59.2	23.3	21.7

[a]The uncertainty of this energy is ±0.2 keV.
[b]The uncertainty of this energy is ±1.0 keV.
[c]The uncertainty of this linewidth is ±1.0 keV.
[d]All of the $\Delta n = 1$ transitions from 2→1 to 6→5 contribute to this peak.

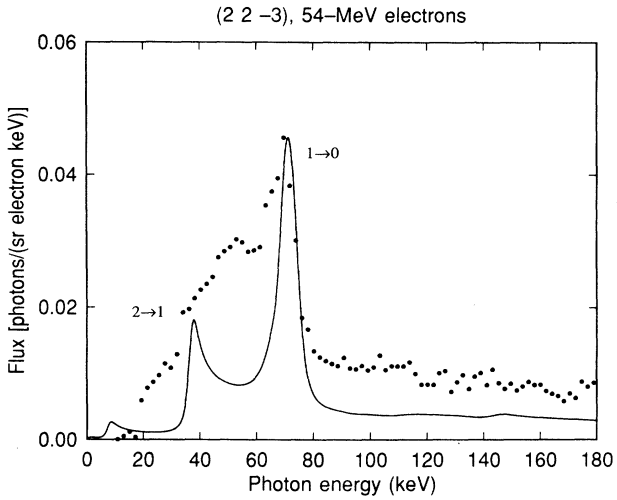

FIG. 13. 54-MeV ($\gamma=106.9$) electrons channeled along the (22−3) plane. Experimental spectrum.

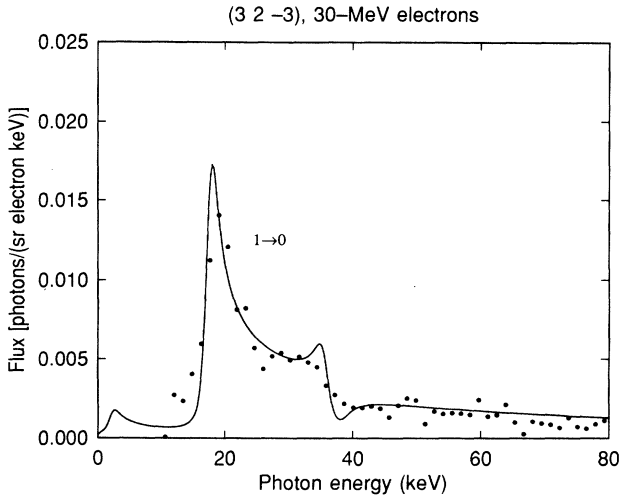

FIG. 14. 30-MeV ($\gamma=60.22$) electrons channeled along the (32−3) plane. Experimental spectrum.

D. Axial channeling-radiation data

Figures 23–26 present the experimental spectra for electrons channeled nearly parallel to the ⟨223⟩ axis, at 30 MeV ($\gamma=60.22\pm0.15$) (Fig. 23) and at 54 MeV ($\gamma=106.9\pm0.3$) (Fig. 24), and nearly parallel to the ⟨001⟩ axis, at 52 MeV ($\gamma=103.0\pm0.3$) (Fig. 25) and at 17 MeV ($\gamma=34.76\pm0.16$) (Fig. 26). Coupling of the particle wave functions to planes that intersect at the axis under study can give planar channeling-radiation lines superimposed on the axial spectra. Figure 23 shows spectral lines at about the same energy as those of Fig. 3, which corresponds to channeling radiation along the (1−10) plane.

Finally, Fig. 27 presents the spectrum for 54-MeV positrons ($\gamma=106.9\pm0.4$) channeled parallel to the ⟨223⟩ axis. The energies of the spectral peaks for axial channeling radiation are given in Table III.

V. DISCUSSION

A. Thermal vibration amplitudes

Table IV shows the present results (far right column) for thermal vibration amplitudes, which compare well with recent values in the literature. If we average our measured vibrational amplitudes for the three axes, we

TABLE II. Peak energies and linewidths of the positron-channeling-radiation spectra. There is some disagreement for the transition energies for 83 MeV for the (21−2) and (10−1) planes.

Plane and beam energy (MeV)	Calculated photon energy (keV) ±0.25 keV	Observed photon energy (keV) ±1.0 keV	Calculated linewidth (keV) ±0.25 keV	Observed linewidth (keV) ±1.0 keV
(1−10)				
54	55.8	55.9	7.5	8.4
83	101.2	101.8	20.5	21.7
(21−2)				
54	56.8[a]	56.9	6.0	9.8
83	101.1	105.8	23.0	20.3
(10−1)				
54	50.8[a]	51.0	5.3	7.0
83	89.6[a]	94.0	19.5	16.8
(32−3)				
83	105.1[a]	108.0	28.0	25.0[b]

[a]Photon energy for transitions between lowest levels, 1→0 and 2→1.
[b]The uncertainty of this linewidth is ±5.0 keV.

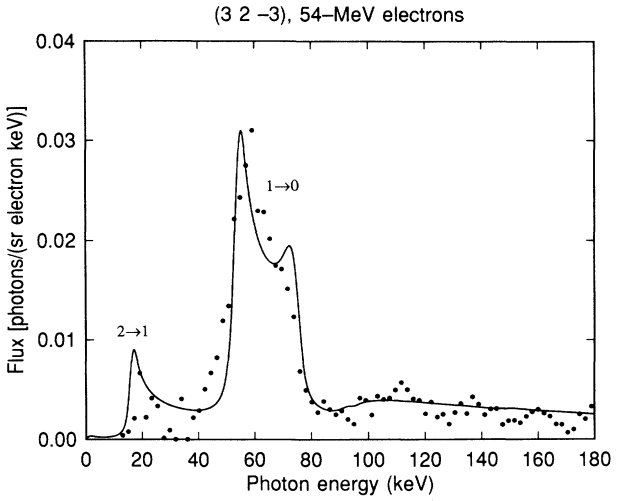

FIG. 15. 54-MeV ($\gamma=106.9$) electrons channeled along the (32−3) plane. Experimental spectrum.

TABLE III. Peak energies and linewidths of the axial channeling-radiation spectra.

Axis and beam energy (MeV)	Type of beam	Observed photon energy (keV)	Observed linewidth (keV)
⟨223⟩			
30	e^-	20.4±0.7	[a]
		28.2±0.7	8.4±0.7
		48.5±0.7	12.0±0.7
		94.7±0.7	[a]
		98.9±0.7	[a]
54	e^-	57.1±1.0	17±1[b]
		124.3±2.0	[c]
		183±7	[c]
54	e^+	55.6±0.8	12±0.8
⟨001⟩			
52	e^-	82.7±3.6	[b]
17	e^-	18.0±0.8	6.0±0.8
		33.9±0.8[b]	[c]
		43.5±0.8[b]	[c]

[a]Not enough data points to state a result.
[b]Inaccuracy is probably larger.
[c]Too much noise to state a value.

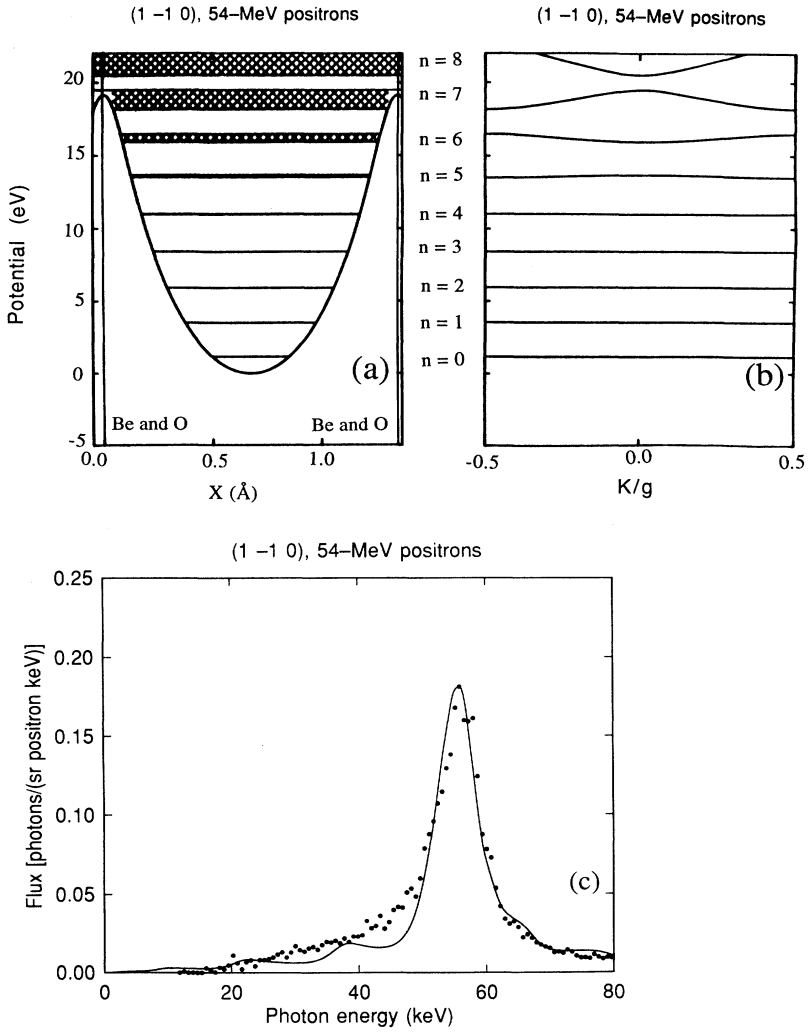

FIG. 16. 54-MeV ($\gamma=106.9$) positrons channeled along the (1−10) plane of BeO. (a) Calculated interplanar potential and energy levels. Vertical lines indicate the position of the atomic planes. Higher-energy levels are broadened in momentum space, due to the presence of neighboring atoms, thus giving an energy band [see also (b)]. (b) Energy vs momentum [$E(\kappa)$] dispersion diagram reduced to the first Brillouin zone (κ is the transverse crystal momentum and **g** the shortest reciprocal-lattice vector perpendicular to the channeling plane). (c) Channeling-radiation spectrum; the dots represent the experimental data points, while the solid line represents the calculated spectrum. Positrons move in a quasiharmonic potential, thus giving almost equal photon energies for transitions starting at different energy levels. Due to linewidth, detector resolution, and Doppler broadening, only one broad line can be observed.

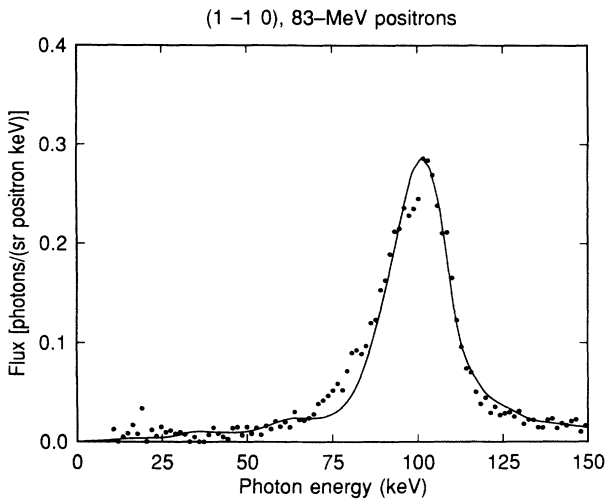

FIG. 17. 83-MeV ($\gamma=162.0$) positrons channeled along the (1−10) plane. Experimental spectrum.

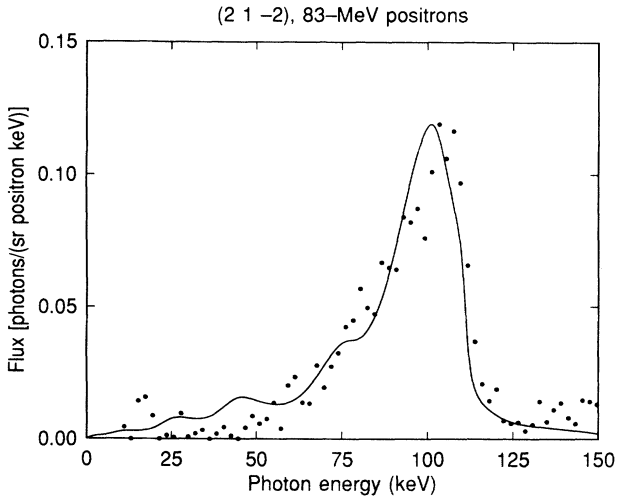

FIG. 19. 83-MeV ($\gamma=162.0$) positrons channeled along the (21−2) plane. Experimental spectrum.

obtain 0.064±0.012 Å for Be and 0.058±0.006 Å for O, in agreement with other studies. No plane that lies nearly perpendicular to the **c** axis was studied, and this accounts for the large uncertainties in the thermal vibration amplitudes along this direction.

B. Electron planar channeling radiation

The background radiation between the channeling-radiation peaks results from transitions between levels above the potential well (free-to-free transitions) and from levels above to levels within the well (free-to-bound transitions). Their broadband nature is due to the energy-momentum dispersion in the Brillouin zone.

At 54 MeV, the (21−2) spectrum contains a 2→0 transition line (Fig. 7). Transitions that are forbidden by symmetry in simpler crystal structures can exist in BeO because the potential wells of the (21−2) and other planes are not symmetric. (See, e.g., Fig. 10.)

Table I compares the calculated and experimental transition energies and linewidths for planar electron channeling along the principal planes. We see that the agreement in general is very good. The few existing discrepancies are discussed below.

Spectral data for 30-MeV electrons channeled along the (21−2) plane (Fig. 6) show the 2→1 transition almost as prominent as the 1→0 transition, in disagree-

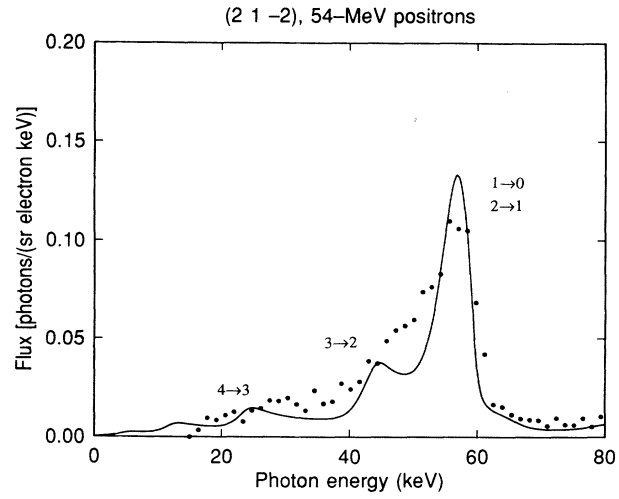

FIG. 18. 54-MeV ($\gamma=106.9$) positrons channeled along the (21−2) plane. Experimental spectrum.

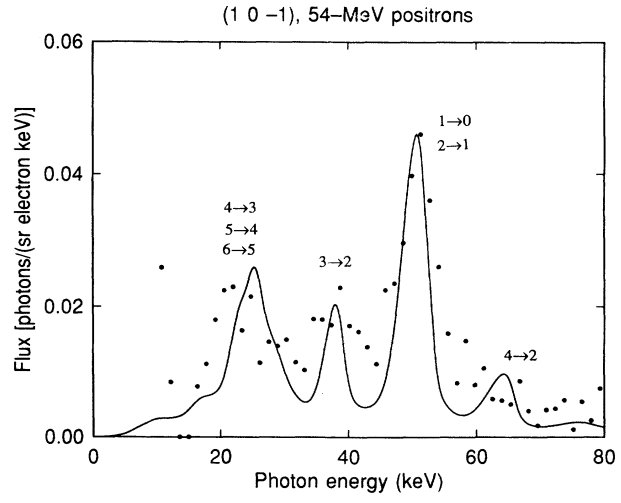

FIG. 20. 54-MeV ($\gamma=106.9$) positrons channeled along the (10−1) plane. Experimental spectrum.

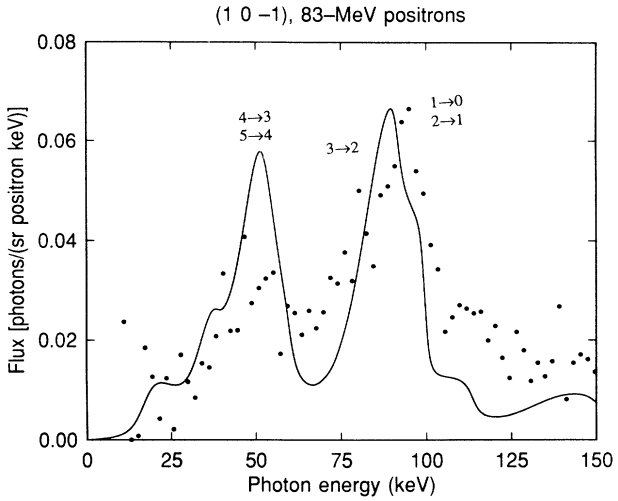

FIG. 21. 83-MeV ($\gamma=162.0$) positrons channeled along the (10−1) plane. Experimental spectrum.

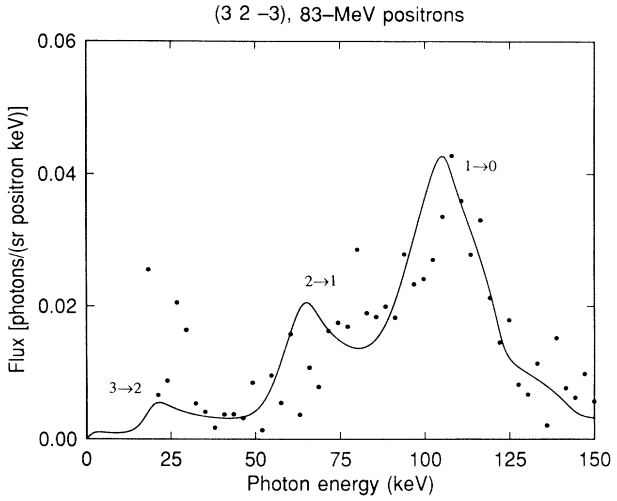

FIG. 22. 83-MeV ($\gamma=162.0$) positrons channeled along the (32−3) plane. Experimental spectrum.

ment with theory. However, the 1→0 transition is characterized by a linewidth much larger than the theoretical one. It is possible that multiple scattering was not well accounted for.[10,11,20] Referring to Table I, the ratio of the experimental linewidth to the theoretical linewidth for the 1→0 transition is about 2. Keeping the areas under each transition peak, i.e., the transition strengths, constant, a 1→0 transition twice as broad will have a peak half as tall, which agrees with the 2→1 peak. (We are not concerned about the 2→1 natural linewidth, or about the linewidth increment due to multiple scattering because this transition is strongly Bloch broadened.) This same criterion is valid when applied to other spectra. For example, for 30-MeV electrons channeled along the (1−10) plane [Fig. 3(c)], if we compare the area under the 1→0 peak to the area under the 3→2 peak, we find about the same situation.

The (100) spectra show, mainly at 17 MeV (Fig. 9), a clear disagreement in the 3→0 transition. The thermal vibration amplitudes $\langle u^2\rangle^{1/2}$ cannot be modified, in par-

TABLE IV. Thermal vibration amplitudes at room temperature of BeO, obtained by different research groups, and their spatial average. (Reference 15 presents two results, which depend on the assumptions made in order to process the data.) The far right column shows our results, with the respective errors. $\langle u_{11}^2\rangle^{1/2}$, thermal vibration amplitude in the x-y plane (for Be or O); $\langle u_{33}^2\rangle^{1/2}$, thermal vibration amplitude in the z direction (for Be or O). The first two lines of data represent a volume average, calculated as $\langle u^2\rangle^{1/2}=\sqrt{(1/3)*(2*\langle u_{11}^2\rangle+\langle u_{33}^2\rangle)}$ for both Be and O. X, x-ray diffraction; n, neutron diffraction; γ, γ-ray diffraction; sc, single crystal; pw, powder; thy, theoretical; mp, multipole analysis; cr, channeling radiation.

Reference:	14	15	16	12	17	18	This
Year:	1956	1964	1964	1972	1985	1987	study
$\langle u_{Be}^2\rangle^{1/2}$ (Å)	0.084	0.088	0.068	0.058	0.066	0.067	0.064
		0.082					±0.012
$\langle u_{O}^2\rangle^{1/2}$ (Å)	0.056	0.078	0.065	0.058	0.057	0.059	0.058
		0.071					±0.006
$\langle u_{Be\ 11}{}^2\rangle^{1/2}$ (Å)	0.087				0.067	0.064	0.0600
							±0.0060
$\langle u_{O\ 11}^2\rangle^{1/2}$ (Å)	0.058				0.057	0.059	0.0580
							±0.0032
$\langle u_{Be\ 33}^2\rangle^{1/2}$ (Å)	0.082				0.064	0.073	0.070
							±0.025
$\langle u_{O\ 33}^2\rangle^{1/2}$ (Å)	0.050				0.057	0.060	0.058
							±0.011
Method	X-sc	X-sc	n-pw	thy	γ,n-sc	X-mp	cr

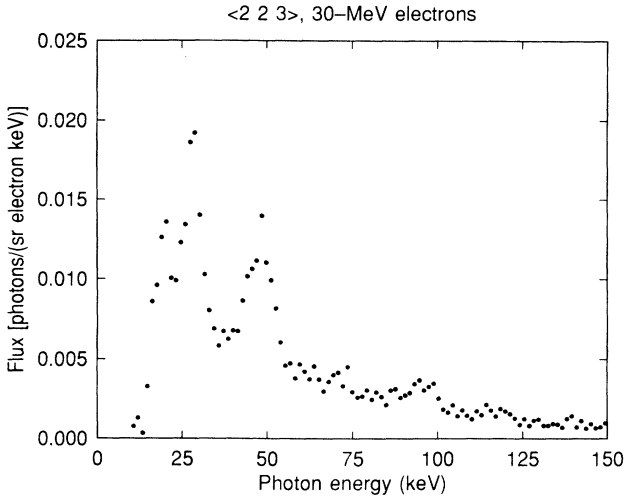

FIG. 23. 30-MeV ($\gamma=60.22$) electrons channeled along the ⟨223⟩ axis. Experimental spectrum.

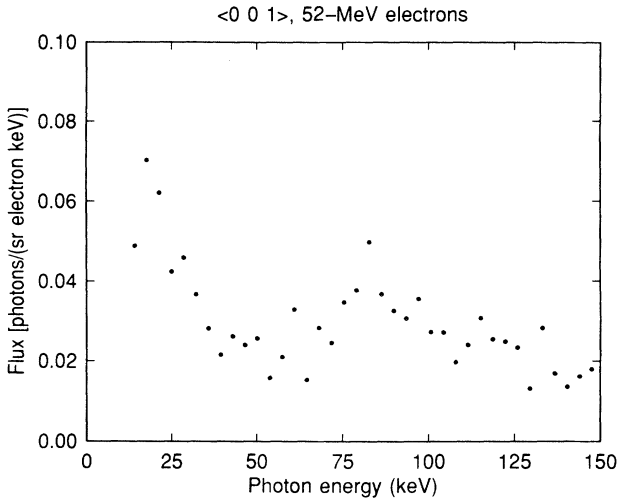

FIG. 25. 52-MeV ($\gamma=103.0$) electrons channeled along the ⟨001⟩ axis. Experimental spectrum.

ticular, increased. We got a good match for the principal planes at 30 and 54 MeV. Furthermore, a modification of $\langle u^2\rangle^{1/2}$ gives, for the (100) plane, about the same change in photon energy for both the $2\rightarrow1$ and $3\rightarrow0$ transitions. For example, a 0.01-Å increase in both $\langle u^2_{\mathrm{Be}}\rangle^{1/2}$ and $\langle u^2_{\mathrm{O}}\rangle^{1/2}$ produces a shift of about -0.5 keV *for both* the $2\rightarrow1$ and $3\rightarrow0$ transitions, at 17 MeV. Modification of the amount of multiple scattering does not affect the spectral energies. It does not appear possible that the electronic cloud distribution, which is due to bonds, changes the crystal potential significantly. Experimental data on x-ray scattering factors for BeO were used instead of the theoretical Hartree-Fock atomic form factors $f_e(s)$.[18] In addition, previous x-ray-diffraction studies indicate that $Be^{+2}O^{-2}$ is a better model than neutral BeO.[14,15,18] Even though the spectra are slightly shifted in energy, applying the same algorithm to the principal planes gives about the same photon energy shift. Taking into account the possibility of inaccurate x-ray measurements and the disagreement between investigators on the ionization percentage,[14,15,18] we decided to retain a uniform theoretical $f_e(s)$ throughout this study. Therefore, we have no explanation for this discrepancy.

Some of the Bloch-broadened transitions are measured to have sharper peaks than theory predicts, e.g., for the $(1-10)$ plane, the $3\rightarrow2$ and the $4\rightarrow3$ transitions at, respectively, 30 MeV [Fig. 3(c)] and 54 MeV (Fig. 4). This fact was also suggested by the electron- and positron-channeling radiation from diamond.[26] Planes with high Miller indices, e.g., $(22-3)$ at 30 MeV (Fig. 12) and

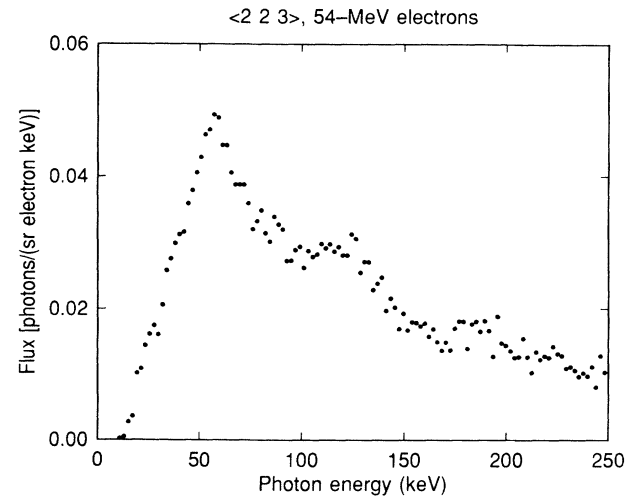

FIG. 24. 54-MeV ($\gamma=106.9$) electrons channeled along the ⟨223⟩ axis. Experimental spectrum.

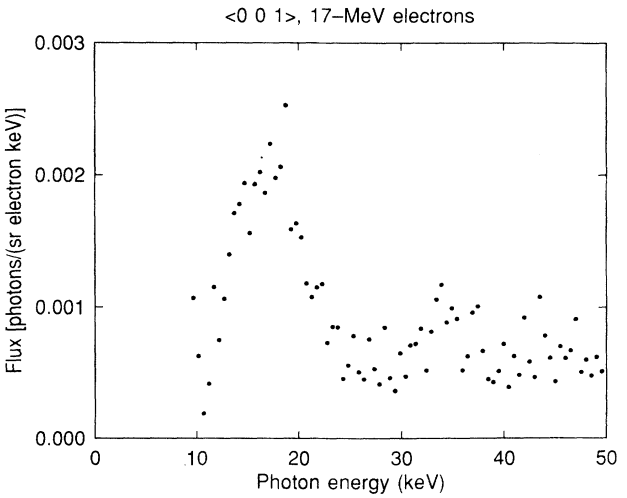

FIG. 26. 17-MeV ($\gamma=34.76$) electrons channeled along the ⟨001⟩ axis. Experimental spectrum.

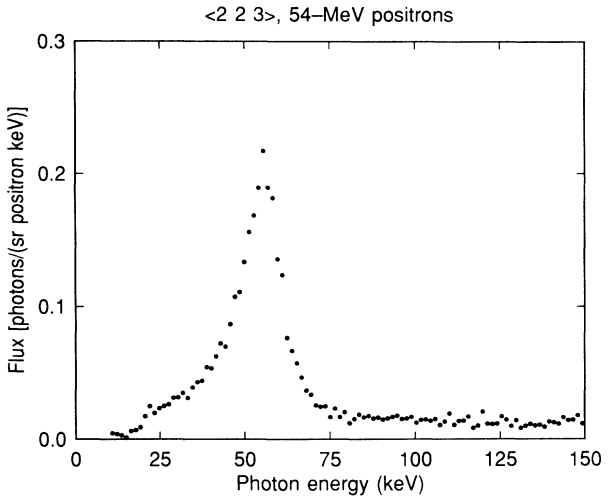

FIG. 27. 54-MeV ($\gamma = 106.9$) positrons channeled along the $\langle 223 \rangle$ axis. Experimental spectrum.

(32−3) at 54 MeV (Fig. 15), show disagreement in their channeling spectra. Once again, no small change in the $\langle u^2 \rangle^{1/2}$ nor in multiple scattering can account for these discrepancies. It is possible, however, that the coupling of the electron wave functions to nearby planes or axes might produce this anomaly. It may also be that the linewidth theory used in this work needs further development.

Another explanation for this anomaly is the possibility of unequal population distribution in the Brillouin zone. Planar channeling is considered here to be a one-dimensional problem, and this gives a constant density of states in κ space. States can be occupied or vacant. Previous experiments suggest that levels, at least inside the well, are equally populated. This can be seen in the analysis of channeling along planes with low Miller indices, e.g., (1−10), Figs. 3(c) and 4. The theoretical method assumes the levels to be populated equally, and the fit to the experimental spectra is good. This is in agreement with the results of channeling in other crystals (see, e.g., Ref. 9). Hence, within each level, because the change in transverse energy is small, no asymmetric population distribution should exist. However, other data are only suggestive, and this is the first study of BeO.

Still another possible explanation is based on a transient situation: during the first few microns inside the crystal, a well-collimated beam populates only one portion of the Brillouin zone. As the particle travels through the crystal, it is scattered, thus changing its transverse energy at other points in the Brillouin zone, and selectively populating higher-energy levels. Therefore, most of the channeling-radiation output would be produced in the first few microns of the crystal, and the observed spectra would depend on the entrance angle.

C. Positron planar channeling radiation

Table II compares the calculated and experimental transition energies and linewidths for positron channeling along the principal planes. The agreement between the theoretical and experimental photon energies is generally good, and for linewidths the agreement is moderately good. Positrons move in an almost harmonic potential, giving nearly equally spaced energy levels. Thus, the transition energies are nearly equal, and only one spectral peak is produced.

There is a slight disagreement in the (21−2) planar spectra at 54 MeV (Fig. 18) and at 83 MeV (Fig. 19) for the shape of the former and the location of the latter. These slight discrepancies may be due to the fact that we do not have the relative strengths of the various transitions quite right. The (1−10) spectral data are fitted very well.

Figure 21 shows the spectrum for 83-MeV positrons channeled along the (10−1) plane. There are discrepancies for both peaks, which may be due to the proximity of the $\langle 233 \rangle$ axis. The same comments on Bloch-broadened states apply here as for electron channeling.

VI. CONCLUSIONS

We have presented a study of electron- and positron-channeling radiation for BeO. Thermal vibration amplitudes were deduced, and agree with the latest values presented in the literature, obtained using different probes.

For narrow-band states, the standard theory gives good agreement with the experiment, for both electron- and positron-channeling radiation. For Bloch-broadened states, the agreement is not always as good; a number of possible explanations are proposed, but none is definitive.

ACKNOWLEDGMENTS

This work was supported in part by the Air Force Office of Scientific Research Grant No. F49620-86-K-0015 and the U.S. Department of Energy.

[1]M. A. Kumakhov and R Wedell, Phys. Status Solidi B **84**, 581 (1977).

[2]R. Wedell, Phys. Status Solidi B **99**, 11 (1980).

[3]D. M. Bird and B. F Buxton, Proc. R. Soc. London, Ser. A **379**, 459 (1982).

[4]J. U. Andersen, E. Bonderup, and R. H. Pantell, Annu. Rev. Part. Sci. **33**, 453 (1983).

[5]J. U. Andersen, in *Quantum Theory of Channeling Radiation*, Vol. 165 of *NATO Advanced Study Institute, Series B: Physics*, edited by R. A. Carrigan, Jr. and J. A. Ellison (Plenum, New York, 1987).

[6]M. A. Kumakhov, in *Proceedings of the First International*

Conference on Coherent Radiation Processes in Strong Fields, Washington, D.C., 1990, edited by V. L. Jacobs, R. Fusina, A. W. Sáenz, and H. Überall [Radiat. Eff. Def. Solids **122-123**, 329 (1991)].

[7]B. L. Berman, in *Proceedings of the First International Conference on Coherent Radiation Processes in Strong Fields* (Ref. 6), p. 277.

[8]A. I. Akhiezer and N. F. Shul'ga, Nucl. Instrum. Methods Phys. Res. B **67**, 262 (1992).

[9]B. L. Berman, J. O. Kephart, R. H. Pantell, S. Datz, H. Park, R. K. Klein, and B. A. Dahling, *Channeling Radiation Experiments between 10 and 100 MeV,* Vol. 165 of *NATO Advanced Study Institute, Series B: Physics,* edited by R. A. Carrigan, Jr. and J. A. Ellison (Plenum, New York, 1987).

[10]J. O. Kephart, R. H. Pantell, B. L. Berman, S. Datz, H. Park, and R. K. Klein, Phys. Rev. B **40**, 4249 (1989).

[11]J. O. Kephart, B. L. Berman, R. H. Pantell, S. Datz, R. K. Klein, and H. Park, Phys. Rev. B **44**, 1992 (1991).

[12]A. Hewat, J. Phys. C **5**, 1309 (1972).

[13]R. W. G. Wyckoff, *Crystal Structures* (Wiley, New York, 1963).

[14]G. A. Jeffrey, G. S. Parry, and R. L. Mozzi, J. Chem. Phys. **25**, 1024 (1956).

[15]D. K. Smith, H. W. Newkirk, and J. S. Kahn, J. Electrochem. Soc. **111**, 78 (1964).

[16]A. W. Pryor and T. M. Sabine, J. Nucl. Mater. **14**, 275 (1964), as quoted in Ref. 10.

[17]J. W. Downs, F. K. Ross, and G. V. Gibbs, Acta Crystallogr. B **41**, 425 (1985).

[18]G. Vidal-Valat, J. P. Vidal, K. Kurki-Suonio, and R. Kurki-Suonio, Acta Crystallogr. A **43**, 540 (1987).

[19]R. K. Klein, J. O. Kephart, R. H. Pantell, H. Park, B. L. Berman, R. L. Swent, S. Datz, and R. W. Fearick, Phys. Rev. B **31**, 68 (1985).

[20]J. O. Kephart, Ph.D. thesis, Stanford University, 1987.

[21]H. D. Dulman, Ph.D. thesis, Stanford University, 1992.

[22]R. L. Swent, Ph.D. thesis, Stanford University, 1982.

[23]G. Radi, Acta Crystallogr. A **26**, 41 (1970).

[24]L. V. Hau, E. Laegsgaard, and J. U. Andersen, Nucl. Instrum. Methods Phys. Res. B **48**, 244 (1990).

[25]N. W. Ashcroft and N. D. Mermin, *Solid State Physics* (Holt, Rinehart, and Winston, New York, 1976).

[26]R. K. Klein, Ph.D. thesis, Stanford University, 1985.